Journal of Zhejiang University-SCIENCE C (Computers & Electronics)
ISSN 1869-1951 (Print); ISSN 1869-196X (Online)
www.zju.edu.cn/jzus; www.springerlink.com
E-mail: jzus@zju.edu.cn

Image stabilization with support vector machine*

Wen-de DONG, Yue-ting CHEN, Zhi-hai XU, Hua-jun FENG†‡, Qi LI

(*State Key Laboratory of Optical Instrumentation, Zhejiang University, Hangzhou 310027, China*)

†E-mail: fenghj@zju.edu.cn

Received July 3, 2010; Revision accepted Feb. 9, 2011; Crosschecked May 5, 2011

Abstract: We propose an image stabilization method based on support vector machine (SVM). Since SVM is very effective in solving nonlinear regression problems, an SVM model was constructed and trained to simulate the vibration characteristic. Then this model was used to predict and compensate for the vibration. A simulation system was built and four assessment metrics including the signal-to-noise ratio (SNR), gray mean gradient (GMG), Laplacian (LAP), and modulation transfer function (MTF) were used to verify our approach. Experimental results showed that this new method allows the image plane to locate stably on the CCD, and high quality images can be obtained.

Key words: Support vector machine (SVM), Vibration, Displacement, Prediction, Compensation
doi:10.1631/jzus.C1000236 **Document code:** A **CLC number:** TP701

1 Introduction

In remote sensing imaging, disturbance of the payloads results in vibration of the space-borne camera, making the obtained images blurred. One solution to this problem is to detect and compensate for the vibration to stabilize the image plane. Nowadays, various compensation schemes have been adopted in image stabilization systems, e.g., using a precisely controlled tip-tilt mirror to compensate for the vibration (Allard *et al*., 2008), or controlling the movement of the focal plane to compensate for the vibration (Janschek and Tchernykh, 2001). Many restoration algorithms have also been used to convert blurred remote sensing images into clear ones. They can be divided into two categories: blind deconvolution (Ben-Ezra and Nayar, 2003; Fergus *et al*., 2006; Shan *et al*., 2008) and non-blind deconvolution (Dey *et al*., 2006; Yuan *et al*., 2008; Zhang *et al*., 2009).

Research shows that the vibration of the space-borne camera can be regarded as a periodic movement composed of several harmonic vibrations, of which the high frequency components have small amplitudes, while the low frequency components have larger amplitudes. The main frequencies that affect the camera are below 100 Hz (Fisher *et al*., 1990).

The simulation system proposed in this paper adopts a tip-tilt mirror for vibration compensation. The vibration displacements are detected by a high-speed camera. With these displacements, control signals are generated and sent to a piezoelectric controller. Then the mirror is driven to compensate for the vibration. There is a phase delay between detection and compensation, however, which results in a residual vibration. Large residual vibration will severely impact the image quality. Since support vector machine (SVM) has a strong capacity to solve nonlinear regression problems, we designed an algorithm using SVM to predict and pre-compensate for the vibration, in order to eliminate the phase delay. Experimental results show that our SVM-based image stabilization method makes the image plane more stable and improves the quality of the obtained images.

‡ Corresponding author

* Project supported by the National Basic Research Program of China (No. 2009CB724006) and the Major Scientific and Technological Project of Zhejiang Province, China (No. 2008C16018)

2 An introduction to SVM

SVM is a supervised learning method that converts the nonlinear classification or regression problem in a low-dimensional space into a linear problem in a high-dimensional space (Cristianini and Shawe-Taylor, 2000; Sapankevych and Sankar, 2009).

Suppose g: $X\subseteq\mathbb{R}^n\rightarrow\mathbb{R}$ is a linear real-valued function in a high-dimensional space. The input vector $\boldsymbol{x}=(x_1, x_2, \ldots, x_n)^{\mathrm{T}}$ that belongs to X will fall into two categories according to whether $g(\boldsymbol{x})$ is smaller than zero. Since $g(\boldsymbol{x})$ is linear, it can be expressed by

$$g(\boldsymbol{x})=\langle \boldsymbol{w}, \boldsymbol{x}\rangle + b=\sum_{i=1}^{n} w_i x_i + b, \tag{1}$$

where $\boldsymbol{w}$ is an n-dimensional vector, and '$\langle\cdot,\cdot\rangle$' is inner product. $g(\boldsymbol{x})$ can be seen as a separating hyperplane in the high-dimensional space. Fig. 1 shows a simple example.

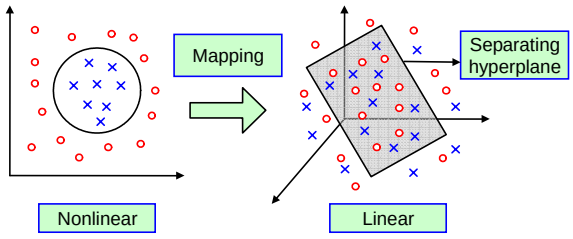

Fig. 1 An example of SVM
'○' stands for $\boldsymbol{x}$: $g(\boldsymbol{x})\geq 0$; '×' stands for $\boldsymbol{x}$: $g(\boldsymbol{x})<0$

In Fig. 1, suppose that the black circle is the solution of a nonlinear classification or regression problem in the 2D space. It is mapped to a separating hyperplane in the 3D space.

We can see that the separating hyperplane is not unique. To determine the optimal one, two definitions must be given first: training set margin and functional margin.

The margin of the training set is defined as half of the Euclidean distance between two points nearest to the separating hyperplane (i.e., the two points are on different sides of the hyperplane). As shown in Fig. 2, γ' denotes the margin of the training set.

Functional margin is defined as $\gamma_i = y_i(\langle \boldsymbol{w}, \boldsymbol{x}_i\rangle + b)$, $\boldsymbol{x}_i\in\mathbb{R}^n$, $y_i\in\{-1, 1\}$. $\gamma_i>0$ means $\boldsymbol{x}_i$ is correctly classified. The goal of SVM is to find the largest margin of the training set while the smallest functional margin is fixed. Lagrangian theory can be used to solve this problem.

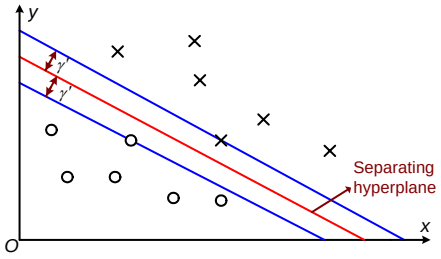

Fig. 2 Margin of the training set
'○' stands for $\boldsymbol{x}$: $g(\boldsymbol{x})\geq 0$; '×' stands for $\boldsymbol{x}$: $g(\boldsymbol{x})<0$. γ' denotes the margin of the training set

If we assume that the function $h(\boldsymbol{x})$ is mapped to $g(\boldsymbol{x})$ by SVM, then Mercer's theorem (Cristianini and Shawe-Taylor, 2000) ensures that $h(\boldsymbol{x})$ can be expressed as a weighted sum of kernel function:

$$h(\boldsymbol{x})=\sum_{i=1}^{l} y_i a_i K(\boldsymbol{x}_i, \boldsymbol{x}) + b, \tag{2}$$

where K denotes the kernel function, and a_i is the weight for $K(\boldsymbol{x}_i, \boldsymbol{x})$. There are several specific forms of kernel function, such as $K(\boldsymbol{x}_i, \boldsymbol{x}_j)=\exp(-\|\boldsymbol{x}_i-\boldsymbol{x}_j\|^2/\sigma^2)$. For more details about SVM theory, please refer to Cristianini and Shawe-Taylor (2000).

3 Vibration prediction and compensation with SVM

3.1 Simulation system

To test our approach, we built a simulation system. Fig. 3 is the schematic diagram. For the spaceborne camera, the imaging distance is so large that the object can be regarded as having an infinite distance, such that the incident line is parallel to the optical axis. To imitate this situation, the target image is put on the focus of the left collimator. After two reflections, the parallel light goes into another collimator on the right, which is put in front of the imaging CCD to form a long focal length imaging system. The detection camera is a high-speed CCD used to obtain the vibration displacements with a detection algorithm, and the calculated data are sent to the computer to generate control signals with SVM. With these signals, the

tip-tilt mirror is driven by the piezoelectric controller to compensate for the vibration. In our system, motion of the object is simulated by vibrating a target image that is put on a high-precision piezoelectric translation stage. Fig. 4 shows part of the target image taken by the imaging CCD. Fig. 5 is the framework of the whole system. We can see that all the components form an open loop.

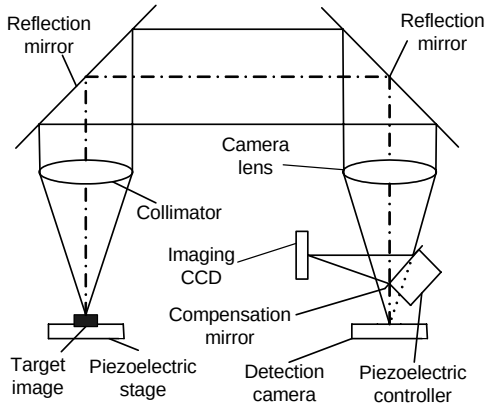

Fig. 3 Simulation system for vibration prediction and compensation

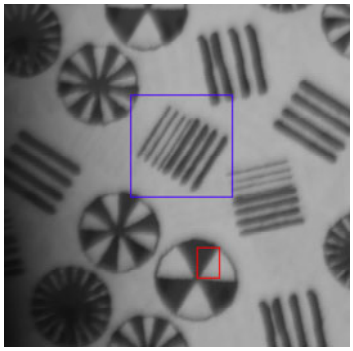

Fig. 4 The target image

The part in the large square will be used in Fig. 11 and the part in the small rectangle will be used in Fig. 12

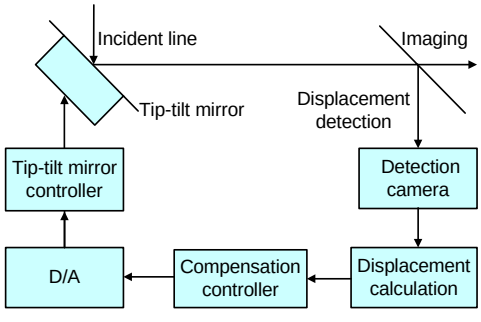

Fig. 5 Framework of the whole system

3.2 Our approach

As mentioned in Section 1, phase delay between detection and compensation results in a residual vibration of the image plane. A large phase delay will seriously degrade the obtained image. Our idea is to predict the vibration displacement with SVM and use the predicted data to pre-compensate for the vibration.

We denote the sampled data set acquired by the detection camera as X'. Since the vibration of the camera subjects to some inherent laws, each $x_n \in X'$ has a relationship with the previously obtained data: x_{n-m}, x_{n-m-1}, …, $x_{n-m-k+1}$. The relationship can be described by the following equation (Shi and Han, 2007; Zhao *et al*., 2008; Kusiak *et al*., 2009):

$$x_n = f(x_{n-m}, x_{n-m-1}, \ldots, x_{n-m-k+1}), \tag{3}$$

where m and k are integers. If f is known, we need only to give a number of k consecutively sampled data to f and obtain an output that indicates the vibration displacement after m sampling intervals. The inputs of f need to be updated continuously in order that the prediction and compensation can be implemented during the whole image stabilization process.

Our approach consists of the following steps:

1. Obtain the training data set: The detection camera obtains hundreds of images of the target image per second. We use a displacement detection algorithm (Lewis, 1995) to calculate the vibration displacements. The calculated displacements form a data set, which is denoted as X'. The data in X' are used to train the SVM model.

2. Construct and train an SVM model: Suppose that we use k consecutively sampled data x_{n-m}, x_{n-m-1}, …, $x_{n-m-k+1}$ to predict the datum x_n after m sampling intervals. According to SVM theory, we must first construct an SVM model with k inputs and one output. We also need to construct a series of training vectors. Each training vector consists of two parts: the input and the output. With an optimization algorithm, the model is trained with the training vectors. The trained model is denoted as G, which is essentially an approximation of f in Eq. (3).

3. Predict and compensate for the vibration displacement: Create a 1D array of size k, and denote the array as 'buffer'. Fill buffer with data $x_{n-m-k+1}$, $x_{n-m-k+2}$, …, x_{n-m}, and then the output $x'_n = G(\text{buffer})$ is the predicted value for x_n. x'_n is used to control the

tip-tilt mirror to compensate for the camera vibration. At the same time, the data in buffer are moved like this: buffer[i]=buffer[i+1] (i=1, 2, …, k−1), and the element in buffer[k] is substituted by a new datum x_{n-m+1}. The prediction and compensation are repeated during the image stabilization process.

Fig. 6 shows an example in which we aim to use five consecutively sampled data to predict the datum after three sampling intervals. For simplicity, we assume that there are only 12 elements (x_1, x_2, …, x_{12}) in the training data set X'. Then we can construct five training vectors (Fig. 6a). With the training vectors and some optimization algorithms (Cristianini and Shawe-Taylor, 2000), the initial SVM model G' is trained. The trained model G is essentially an approximation of function f in Eq. (3) under the condition k=5, m=3.

Fig. 6b shows how G is used for prediction. Suppose that at a certain moment, we import five consecutively sampled data x_n, x_{n+1}, …, x_{n+4} into G to calculate a datum x'_{n+7} (x'_{n+7} is the predicted value for x_{n+7}). Then x'_{n+7} is used to control the vibration compensation system. At the same time, the data in buffer are moved forward, and a new sampled datum x_{n+5} is put in the tail of buffer; the updated data in buffer are imported into G again to do another prediction. The process is repeated during image stabilization.

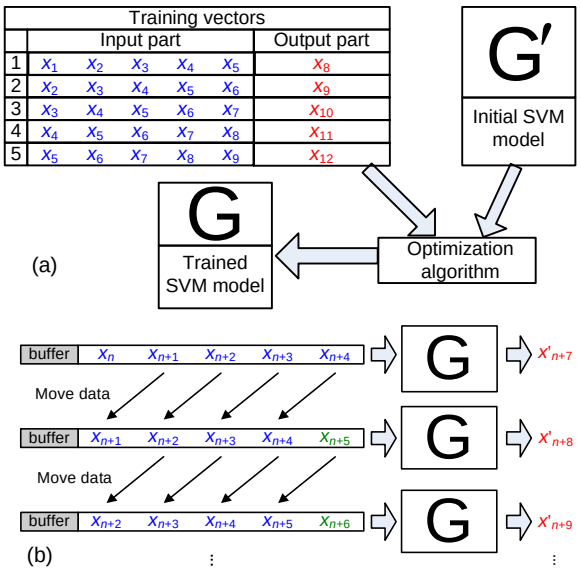

Fig. 6 An example for SVM training and prediction
(a) Training an SVM model with training vectors; (b) Using the trained SVM model to do prediction

3.3 Timing diagram and parameters setting

As Eq. (3) shows, there are two parameters k and m which need to be set, and we empirically set k between 10 and 20. To set m, however, we must learn the scheduling first.

Figs. 7a and 7b are the timing diagrams under two different conditions, where S_0 denotes the moment when the first prediction starts. In our simulation system, the compensation and sampling are controlled such that they are completed at the same time. For example, in Fig. 7a, S_1 is equal to C_1.

Fig. 7a shows the condition where $t_1+t_2<t_0$. During each sampling interval, we need only to predict the datum for the next sampling moment; i.e., P_1 predicts the datum for S_1, P_2 predicts the datum for S_2, and so on. Under this condition, we set m=1.

Fig. 7b shows the condition when $t_0<t_1+t_2<2t_0$. The prediction and compensation cannot be completed within one sampling interval. Thus, we have to abandon the prediction for S_1; i.e., P_1 predicts the datum for S_2, P_2 predicts the datum for S_3, and so on. Under this condition, we set m=2.

For the more general condition, where $(n-1)t_0<t_1+t_2<nt_0$, we have to abandon the predictions for S_1, S_2, …, S_{n-1}; i.e., P_1 predicts the datum for S_n, P_2 predicts the datum for S_{n+1}, and so on. Under this condition, we set m=n.

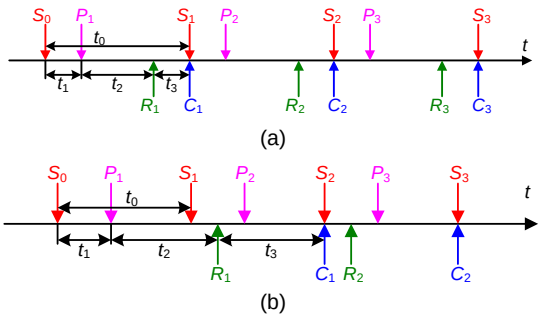

Fig. 7 Timing diagrams under different conditions
(a) $t_1+t_2<t_0$. During each sampling interval, we need only to predict the datum for the next sampling moment. (b) $t_0<t_1+t_2<2t_0$. The prediction and compensation cannot be completed within one sampling interval, and thus the prediction for S_1 is abandoned. For the more general condition, $(n-1)t_0<t_1+t_2<nt_0$, the predictions for S_1, S_2, …, S_{n-1} are abandoned. S: the moment when the sampling is completed; P: the moment when the prediction is completed; R: the moment when the control signal is ready for compensation; C: the moment when the compensation is completed. t_0: the sampling interval; t_1: the time consumed for completing one prediction; t_2: the time consumed for signal preparation; t_3: the waiting time before compensation

4 Simulation and assessments

4.1 An introduction to our experiment

To imitate the vibration characteristic of the space-borne camera, we designed an experiment in which the target image is vibrated following a given periodic signal. Fig. 8 shows the vibration detected by the detection camera. Since the frame rate of the detection camera is set to be 80 frames/s, the sampling interval is 1/80 s.

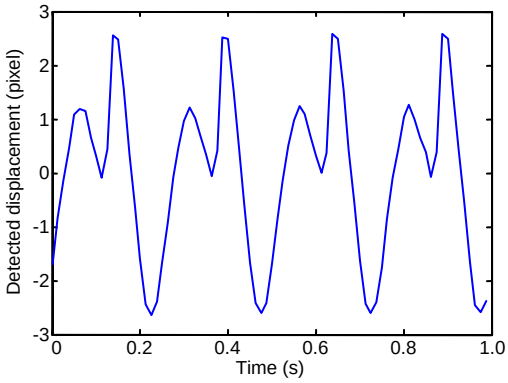

Fig. 8 Vibration detected by the detection camera
For clarity, only four periods are provided here

According to Sections 3.2 and 3.3, we used 12 consecutively sampled data to predict the vibration displacement after two sampling intervals, i.e., k=12, m=2. The SVM model was trained with 200 sampled data. The training time is less than 0.5 s and the average time for predicting once is 0.05 ms (computer configuration: Intel® Xeon® CPU E5404 2 GHz, 4 GB DDRII memory, Microsoft Windows 2003).

To verify the effectiveness of our approach, we compared the performances of the simulation system under three different conditions: taking the image without vibration prediction or compensation; taking the image with vibration compensation only; and, taking the image with both vibration prediction and compensation. The results are given in the following.

4.2 Experimental results and analysis

If we compensate for the vibration without prediction, then the detected vibration displacement is used directly to control the tip-tilt mirror. Since the system needs some time to prepare control signal and rotate the tip-tilt mirror, there is a phase delay between the vibration and compensation.

Fig. 9a imitates the negative effect caused by the phase delay. The dashed curve denotes the vibration detected by the detection camera, the solid curve denotes the compensation signal, and Δt=0.025 s is the assumed phase delay. We can obtain that at t=0.3 s, the compensation displacement is x_1=−0.1699 while the vibration displacement is x_2=0.9590, so there remains a difference Δx=1.1289 which cannot be compensated. If the vibration is of low frequency and the detection frequency is high enough, Δx will be so small that it does not affect the result too much. However, if the vibration frequency is high and the detection frequency is relatively low, Δx will be large and severely impact the image stabilization.

In Fig. 9b, the dashed curve denotes the detected vibration, while the solid curve denotes the compensation signal with SVM prediction. We can see that, although there are some small differences between the two curves, the phase delay disappears.

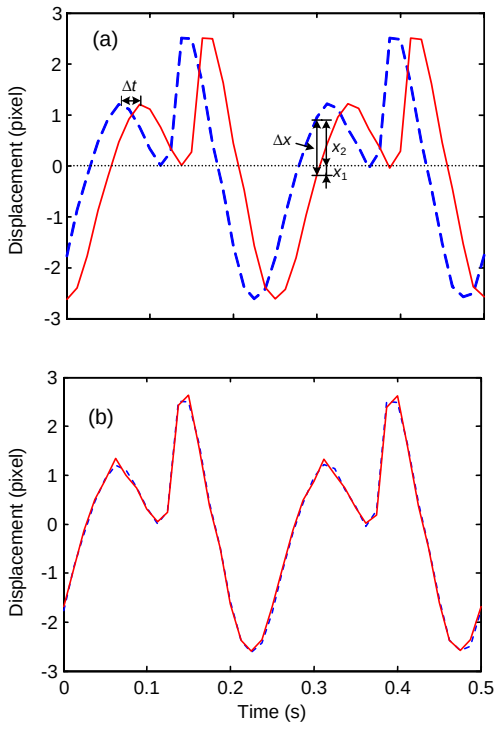

Fig. 9 The negative effect caused by phase delay (a) and the vibration compensation with prediction (b)
The dashed curve denotes the detected vibration, and the solid curve denotes the compensation signal. In (a), Δt=0.025 s is the assumed phase delay. There remains a difference Δx=1.1289 which cannot be compensated

Fig. 10 shows the error curve and the histogram between the dashed and solid curves in Fig. 9b. The maximum absolute error is less than 0.2 pixels and more than 80% of the error data are between −0.15 and 0.15 pixels. This accuracy is high enough for image stabilization.

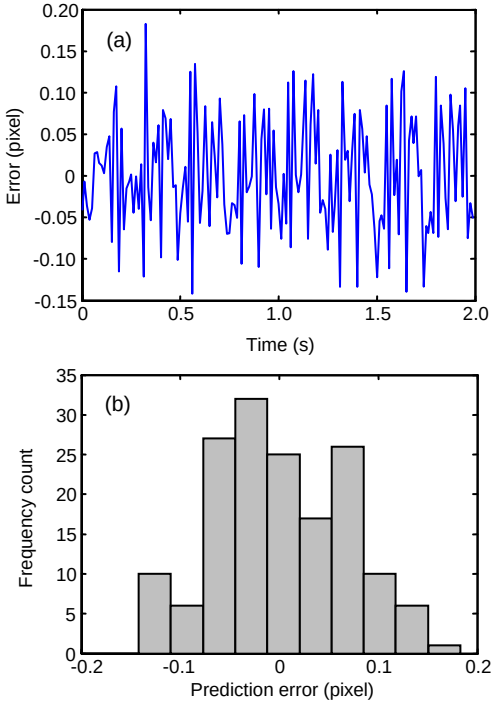

Fig. 10 The error curve between the predicted displacements and the detected displacements (a) and the error histogram (b)

In simulations, the performances of the simulation system under different conditions are compared:

1. Without prediction or compensation, the image displayed on the computer screen vibrates with a large amplitude.

2. With compensation only, because of the phase delay, there is still an apparent residual vibration of the image.

3. With both prediction and compensation, the image is almost motionless on the computer screen.

Since vibration results in a blurred image, the clearness of the image can be used to measure the vibration: the clearer the image is, the smaller the vibration is. Fig. 11 shows four images taken under different conditions.

Since Fig. 11d is taken when the target image is still, it is the clearest. Fig. 11a is taken when there is no vibration compensation, so it is the most blurred. Fig. 11b is also blurred because there is a large phase delay. Fig. 11c is of higher quality than Fig. 11b because the vibration prediction eliminates the negative effects caused by phase delay.

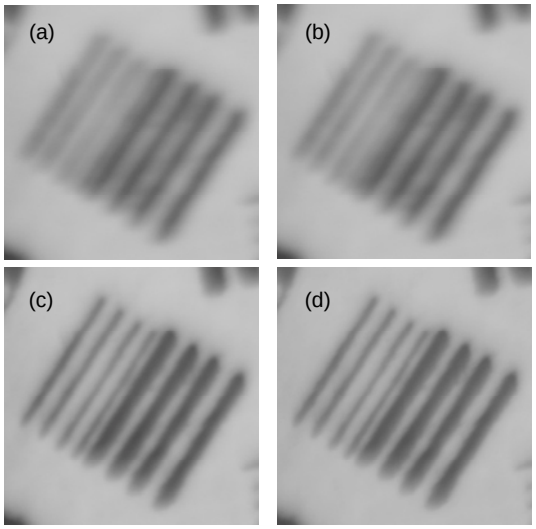

Fig. 11 Images taken under different conditions (zoom of the part in the large square of Fig. 4)
(a) Without prediction or compensation; (b) With compensation only; (c) With both prediction and compensation; (d) With no vibration (the target image is still)

We used three image quality assessment metrics to assess the images mathematically: one is the signal-to-noise ratio (SNR), which is widely used to measure the pixel value difference between the reference image and the test image; the other two are the gray mean gradient (GMG) and the Laplacian (LAP) (Feng *et al*., 2010), which are used to measure the textures of the image. Images with finer textures will receive higher scores. The definitions of the three metrics are given in Eqs. (4)–(6). The results are shown in Table 1.

$$\mathrm{SNR}=10\lg\left(\|\boldsymbol{o}\|^2/\|\boldsymbol{g}-\boldsymbol{o}\|^2\right), \tag{4}$$

$$\mathrm{GMG}=\frac{1}{(M-1)(N-1)}\sum_{i=1}^{M-1}\sum_{j=1}^{N-1}\left\{\frac{1}{2}\left\{[g(i+1,j)-g(i,j)]^2+[g(i,j+1)-g(i,j)]^2\right\}\right\}^{1/2}, \tag{5}$$

$$\mathrm{LAP}=\frac{1}{(M-2)(N-2)}\sum_{i=2}^{M-1}\sum_{j=2}^{N-1}\left|8g(i,j)-g(i-1,j-1)-g(i-1,j)-g(i-1,j+1)-g(i,j-1)-g(i,j+1)-g(i+1,j-1)-g(i+1,j)-g(i+1,j+1)\right|, \tag{6}$$

where $\boldsymbol{g}$ and $\boldsymbol{o}$ denote the test image and reference image (Fig. 11d), respectively, and M and N denote the numbers of rows and columns of the images, respectively.

Table 1 Results of image assessment metrics

Figure	SNR (dB)	GMG	LAP
11a	15.0236	0.8630	2.5758
11b	15.0930	0.8783	2.5808
11c	15.4314	1.0039	2.7396
11d	∞	1.0052	2.8907

SNR: signal-to-noise ratio; GMG: gray mean gradient; LAP: Laplacian

From Table 1, we see that except the reference image in Fig. 11d, Fig. 11c is of the highest quality—its assessment scores are very close to those of the reference image. The scores of Fig. 11b, however, are only a little higher than those of the blurred image shown in Fig. 11a. The results mean that there remains a large residual vibration in Fig. 11b due to the phase delay, and in Fig. 11c the phase delay is significantly reduced with our approach.

Besides SNR, GMG, and LAP, we also calculated the modulation transfer function (MTF) (Goodman, 2004) with the slanted-edge method (ISO 12233:2000). MTF has been used widely to characterize and quantify the spatial frequency response of an imaging system. It is defined as the contrast ratio between a given spatial frequency and the fixed low spatial frequency. Thus, at a given spatial frequency f, higher MTF means higher contrast. Fig. 12 exhibits the images (the part in the small rectangle of the target image) with which the MTF values were calculated.

Fig. 13 shows the MTF curves calculated under different conditions. Within the cut-off spatial frequency, the optical system is of the lowest MTF when there is no vibration compensation. With compensation only, the MTF is only a little higher, which means the vibration is not efficiently compensated. With both vibration prediction and compensation, the MTF is much improved and is very close to that when the target image is still, which means the vibration has been significantly compensated for. The MTF values at a given frequency f are shown in Fig. 13.

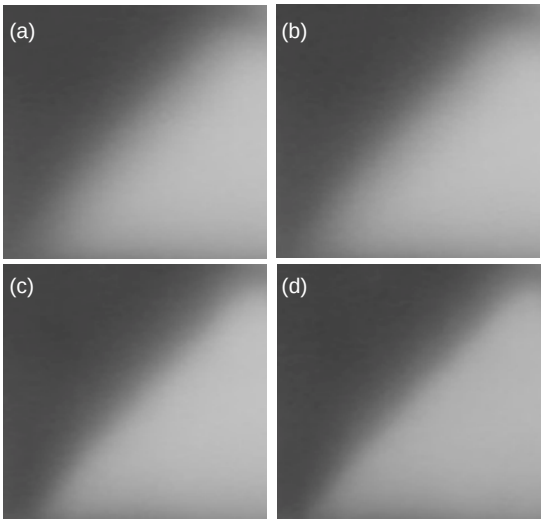

Fig. 12 Zoom of the part in the small rectangle of the target image, which is used to calculate the modulation transfer function (MTF)
(a) With no compensation or vibration; (b) With compensation only; (c) With both prediction and compensation; (d) With no vibration (the target image is still)

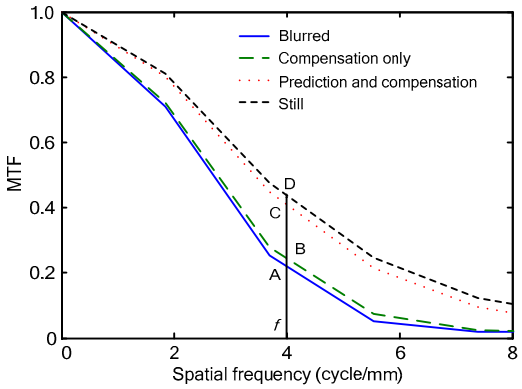

Fig. 13 Modulation transfer function (MTF) calculated under different conditions
At the given f, the MTF values are: A, 0.2527; B, 0.2779; C, 0.4475; D, 0.4749

5 Conclusions

This paper presents a new image stabilization method for the space-borne camera. With an SVM model trained on the sampled data set, we predicted and pre-compensated for the vibration. Experimental results show that the prediction is of high precision and that the image plane is almost motionless after vibration compensation. To further verify the

effectiveness of our method, we used three image quality assessment metrics (SNR, GMG, LAP) to assess the taken images. We also used MTF to compare the system responses under different conditions. Results show that the phase delay with direct vibration compensation almost completely disappears using our SVM-based method and that the quality of the obtained images is improved.

References

Allard, J.P., Chamberland, M., Farley, V., Marcotte, F., Rolland, M., Vallières, A., Villemaire, A., 2008. Airborne measurements in the longwave infrared using an imaging hyperspectral sensor. *SPIE*, **7086**:70860K-1-70860K-12. [doi:10.1117/12.795119]

Ben-Ezra, M., Nayar, S.K., 2003. Motion Deblurring Using Hybrid Imaging. IEEE Computer Society Conf. on Computer Vision and Pattern Recognition, **1**:657-664. [doi:10.1109/CVPR.2003.1211416]

Cristianini, N., Shawe-Taylor, J., 2000. An Introduction to Support Vector Machines and Other Kernel-Based Learning Methods. Li, G.Z., Wang, M., Zeng, H.J., translators, 2004. Publishing House of Electronics Industry, Beijing, China, p.82-109 (in Chinese).

Dey, N., Blanc-Feraud, L., Zimmer, C., Roux, P., Kam, Z., Olivo-Marin, J.C., Zerubia, J., 2006. Richardson-Lucy algorithm with total variation regularization for 3D confocal microscope deconvolution. *Microscopy Res. Techn.*, **69**(4):260-266. [doi:10.1002/jemt.20294]

Feng, H.J., Wang, Y.P., Xu, Z.H., Li, Q., Lei, H., Zhao, J.F., 2010. Real-time deblurring algorithm with robust noise suppression. *J. Zhejiang Univ.-Sci. C (Comput. & Electron.)*, **11**(5):375-380. [doi:10.1631/jzus.C0910201]

Fergus, R., Singh, B., Hertzmann, A., Roweis, S.T., Freeman, W.T., 2006. Removing camera shake from a single photograph. *ACM Trans. Graph.*, **25**(3):787-794. [doi:10.1145/1141911.1141956]

Fisher, M., Hadar, O., Kopeika, N.S., 1990. Numerical calculation of modulation transfer functions for low-frequency mechanical vibrations. *SPIE*, **1342**:72-83. [doi:10.1117/12.23160]

Goodman, J.W., 2004. Introduction to Fourier Optics (3rd Ed.). Robert & Company Publisher, USA, p.127-173.

ISO 12233:2000. Photography-Electronic Still-Picture Cameras-Resolution Measurements. International Organization for Standardization, Geneva.

Janschek, K., Tchernykh, V., 2001. Optical correlator for image motion compensation in the focal plane of a satellite camera. *Space Technol.*, **21**(4):127-132.

Kusiak, A., Zheng, H., Song, Z., 2009. Short-term prediction of wind farm power: a data mining approach. *IEEE Trans. Energy Conv.*, **24**(1):125-136. [doi:10.1109/TEC.2008.2006552]

Lewis, J.P., 1995. Fast Template Matching. Vision Interface, Canadian Image Processing and Pattern Recognition Society, p.120-123.

Sapankevych, N., Sankar, R., 2009. Time series prediction using support vector machines: a survey. *IEEE Comput. Intell. Mag.*, **4**(2):24-38. [doi:10.1109/MCI.2009.932254]

Shan, Q., Jia, J., Agarwala, A., 2008. High-quality motion deblurring from a single image. *ACM Trans. Graph.*, **27**(3). [doi:10.1145/1399504.1360672]

Shi, Z.W., Han, M., 2007. Support vector echo-state machine for chaotic time-series prediction. *IEEE Trans. Neur. Networks*, **18**(2):359-372. [doi:10.1109/TNN.2006.885113]

Yuan, L., Sun, J., Quan, L., Shum, H.Y., 2008. Progressive inter-scale and intra-scale non-blind image deconvolution. *ACM Trans. Graph.*, **27**(3). [doi:10.1145/1399504.1360673]

Zhang, W., Zhao, M., Wang, Z., 2009. Adaptive wavelet-based deconvolution method for remote sensing imaging. *Appl. Opt.*, **48**(24):4785-4793. [doi:10.1364/AO.48.004785]

Zhao, J.H., Zhao, Y.D., Zhao, X., Wong, K.P., 2008. A statistical approach for interval forecasting of the electricity price. *IEEE Trans. Power Syst.*, **23**(2):267-276. [doi:10.1109/TPWRS.2008.919309]